ACCEPTED VERSION

This is the accepted version of the following article:

Shaheer Maher, Denver Linklater, Hadi Rastin, Pei Le Yap, Elena P. Ivanova, and Dusan Losic
Tailoring Additively Manufactured Titanium Implants for Short-Time Pediatric Implantations with Enhanced Bactericidal Activity
ChemMedChem, 2022; 17(2):e202100580-1-e202100580-13

© 2021 Wiley-VCH GmbH

which has been published in final form at http://dx.doi.org/10.1002/cmdc.202100580

This article may be used for non-commercial purposes in accordance with the Wiley Self- Archiving Policy [https://authorservices.wiley.com/author-resources/Journal-Authors/licensing/self-archiving.html].

PERMISSIONS

http://www.wiley-vch.de/cta/physsci-en

COPYRIGHT TRANSFER AGREEMENT

2. Accepted Version. Wiley-VCH licenses back the following rights to the Contributor in the version of the Contribution that has been peer-reviewed and accepted for publication ("Accepted Version"), but not the final version:
a. The right to self-archive the Accepted Version on the Contributor's personal website, in the Contributor's company/institutional repository or archive, in Compliant SCNs, and in not-for-profit subject-based repositories such as PubMed Central, subject to an embargo period of 12 months for scientific, technical and medical (STM) journals following publication of the Final Published Version. There are separate arrangements with certain funding agencies governing reuse of the Accepted Version as set forth at the following website: www.wiley.com/go/funderstatement. The Contributor may not update the Accepted Version or replace it with the Final Published Version. The Accepted Version posted must contain a legend as follows: This is the accepted version of the following article: FULL CITE, which has been published in final form at [Link to final article]. This article may be used for non-commercial purposes in accordance with the Wiley Self-Archiving Policy [https://authorservices.wiley.com/author-resources/Journal-Authors/licensing/self-archiving.html].

14 November 2022

http://hdl.handle.net/2440/133403

Tailoring Additively Manufactured Titanium Implants for Short-Time Pediatric Implantations with Enhanced Bactericidal Activity

Shaheer Maher,[a, b] Denver Linklater,[c] Hadi Rastin,[a] Pei Le Yap,[a] Elena P. Ivanova,[c, d] and Dusan Losic*[a]

Paediatric titanium (Ti) implants are used for the short-term fixation of fractures, after which they are removed. However, bone overgrowth on the implant surface can complicate their removal. The current Ti implants research focuses on improving their osseointegration and antibacterial properties for long-term use while overlooking the requirements of temporary implants. This paper presents the engineering of additively manufactured Ti implants with antibacterial properties and prevention of bone cell overgrowth. 3D-printed implants were fabricated followed by electrochemical anodization to generate vertically aligned titania nanotubes (TNTs) on the surface with specific diameters (~100 nm) to reduce cell attachment and proliferation. To achieve enhanced antibacterial performance, TNTs were coated with gallium nitrate as antibacterial agent. The physicochemical characteristics of these implants assessed by the attachment, growth and viability of osteoblastic MG-63 cells showed significantly reduced cell attachment and proliferation, confirming the ability of TNTs surface to avoid cell overgrowth. Gallium coated TNTs showed strong antibacterial activity against *S. aureus* and *P. aeruginosa* with reduced bacterial attachment and high rates of bacterial death. Thus a new approach for the engineering of temporary Ti implants with enhanced bactericidal properties with reduced bone cell attachment is demonstrated as a new strategy toward a new generation of short-term implants in paediatrics.

Introduction

Titanium (Ti) and its alloys have been widely utilized in pediatrics in the management of bone fractures, trauma or the correction of anatomical deformities (*e.g.*, pins, nails, plates, external fixators or frames).[1] The majority of these implantations in pediatrics requires the removal of the implants after their intended function is fulfilled in order to avoid many complications such as bone growth arrest, bone remodeling, implant fracture upon continuous pressure, implant migration or bone resorption.[2] Other reasons for implant removal also include pain, infection, dislodgement or, in some cases, carcinogenesis.[2c] Given that the implants should be removed, excessive bone growth or attachment onto the implant surface is not desirable and can be a major problem for implants removal leading to increased costs, implant breakage during its removal or excision of bone tissue, which in turn enhances the susceptibility to re-fracture.[2a] Thus, an ideal implant for pediatric applications should not support bone cell overgrowth on its surface, while achieving the desired bone fixation during its short-term application. These requirements are opposite to conventional long-term implants where fast and strong osseointegration, combined with antibacterial protection, are two of the most desirable functions and it is not surprising there is a very limited number of studies on surface modification of Ti to reduce bone growth and osseointegration.

Since the implant surface is the first site of interaction with bone cells, recent studies have confirmed the influence of its surface topography and properties on cells adhesion, proliferation and differentiation.[3] However, the impact of surface roughness (e.g. micro or nano) and surface feature geometry (pores, tubes, particles, rods, wires, spikes etc.) on bone tissue formation is still inconclusive, making it difficult to compare the influence of these topographical features.[3d] For example, Cavalacanti-Adam *et al.* showed that titania nanotubes with diameters ~100 nm can disrupt integrin clusters and thus inhibits cellular adhesion and proliferation.[4] On the other hand, He *et al.* showed that nanopores (30 nm in diameter) promoted cell adhesion and improved healing *in-vivo*.[5] It is important to mention that the majority of the research done so far focused on enhancing cells-surface interaction for the development of implants which remain in the body for an extended period (*e.g.*, hip or knee replacements)[6] with only a few studies involving the design of implants for short-term use.[2c,7]

Bone overgrowth is not the only limitation that affects the performance and functionality of temporary implants in pediatrics; bacterial infection is considered another major

[a] S. Maher, Dr. H. Rastin, Dr. P. Le Yap, Prof. D. Losic
School of Chemical Engineering and Advanced Materials
The University of Adelaide, Adelaide SA 5005 (Australia)
E-mail: dusan.losic@adelaide.edu.au
[b] S. Maher
Faculty of Pharmacy, Assiut University
Assiut, 71526 (Egypt)
[c] Dr. D. Linklater, Prof. E. P. Ivanova
College of STEM, School of Science
RMIT University, Melbourne VIC 3000 (Australia)
[d] Prof. E. P. Ivanova
Australian Research Council (ARC) Training Centre in Surface Engineering for Advanced Materials (SEAM)
Swinburne University of Technology
Hawthorn VIC 3122 (Australia)

© 2021 Wiley-VCH GmbH

problem that could result in implant failure or bone sepsis before complete bone healing is achieved.[6c] Systemic antibiotics administration is the most common practice to prevent and treat implants related bacterial infections.[8] However, the concentration of antibiotic reaching the site of the implant is often inadequate to infiltrate the bacterial biofilm leading to treatment failure.[9] As a result, localized drug delivery through coating of implants with antibiotics seems to be a promising approach.[3a,10] However, the local application of antibiotics at the implant site (*e.g.*, antibiotic-loaded cement) can cause localized cell toxicity and contributes to the development of antibiotic-resistant bacterial strains, such as methicillin-resistant *Staphylococcus aureus* (MRSA).[11] To address the problems of antimicrobial resistance (AMR), considerable research effort has been focused on exploring alternative approaches to conventional Ti implants. Recent advancements in the design of antibacterial Ti biomaterials include incorporating non-conventional metal antibacterial agents such as silver, copper and gallium,[12] altering surface properties such as charge, and hydrophobicity by chemical modification, or engineering of the surface topography,[8,13] physical contact killing of bacteria by sharp surface nanostructures[14] or using drug-releasing titania nanotubes (TNTs) structures loaded with antibacterial drugs.[15]

Additive manufacturing, or 3D-printing technology, has triggered a revolution in the manufacturing sector across various industries including Ti orthopedic and dental implants. Selective laser melting (SLM) is an example of a 3D-printing technique for implant fabrication with the ability to print a variety of metals (*e.g.*, Ti based, stainless steel, Mg, Zn, and Ta) while reducing manufacturing waste and the overall costs of medical implants.[16] SLM can also print metal combinations or metal/ceramic combination implants with no post-processing requirements that are usually necessary for traditional techniques such as casting or machining.[17] More importantly, 3D-printing of the implants provides design flexibility with the ability to fabricate low-cost implants with complex geometries to mimic bone porosity.[18] Moreover, it can offer "on demand" production of implants specifically tailored for children that is fast, and reliable for the best anatomical match using computer-aided design models saving time and costs.[18a,19]

Considering the above discussions, herein, we present a study to demonstrate the design of antibacterial 3D-printed Ti materials for short-term implantations, such as those used in pediatrics, that are able to prevent bacterial infection and reduce excessive cell-surface interaction to allow easier implant removal. To address this challenge, 3D-printed Ti alloy implants with micro-nano hierarchical topographies were fabricated using SLM followed by electrochemical anodization (EA) to generate TNTs on the surface with controlled diameters of 100 nm, which has been shown in previous studies to be optimal for the reduction of cell surface adhesion.[20] To simultaneously enhance the bactericidal properties, the fabricated Ti implants were coated with gallium nitrate. The release of Ga^{3+} is well known to possess strong antibacterial activity based on its ability to interfere with bacterial metabolic activity.[12c] The design and fabrication of the engineered Ti implants is shown schematically in Figure 1. The attachment, proliferation, and viability of osteoblastic MG-63 cells was assessed to evaluate the suitability of the modified Ti topography as a short-term implantable material. Furthermore, the antibacterial activity of Ga^{3+} and TNTs was evaluated against two common human bacterial pathogens; gram-positive *Staphylococcus aureus* and gram-negative *Pseudomonas aeruginosa*.[21] The results of this study provide novel insights into an innovative approach to tailor the surface of Ti implants for temporary or short-term applications, such as those used in pediatric orthopedic surgery, that is currently lacking and urgently needed.

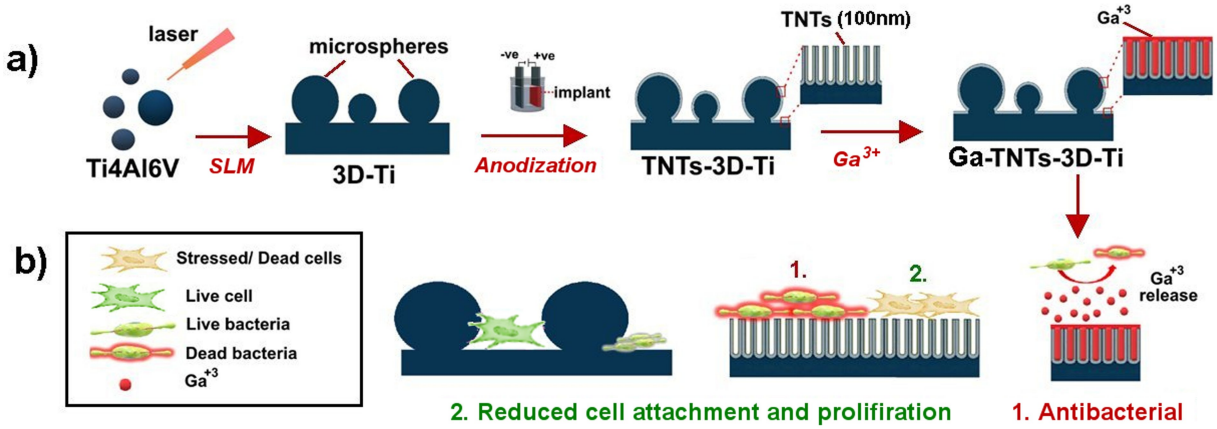

Figure 1. Illustrated representation of 3D-printed Ti implants fabrication by selective laser melting (SLM) followed by electrochemical anodization (EA) to generate a unique surface with microparticles combined with titania nanotubes (TNTs) able to control cells attachment. Ga^{3+} release used to passively kill bacteria in proximity to the implant whereas TNTs effectively reduce bone cell and bacterial attachment. The combination of microsphere and TNTs structures was designed based on the rationale to provide reduced bone cell attachment for short-term implant applications.

© 2021 Wiley-VCH GmbH

Results and Discussion

Characterization of fabricated 3D-printed TNTs implants

To prepare TNTs structures with optimized pore diameters of ~100 nm that could provide reduced cell surface attachment, an initial study using different anodization voltages (20, 40 and 60 V) was performed. During anodization, TNTs were generated on the smooth 3D-Ti surface through etching by fluoride ions under influence of the applied electrical field.[22] SEM images, Figure 2, revealed that the TNTs diameters increased with increased voltage, in agreement with previous reports.[23] TNTs prepared at 60 V for 15 min showed the largest diameter (100 ± 20 nm) compared to those fabricated at 20 and 40 V, Figure 2d, and thus they were selected for further experiments.

The typical surface morphology of 3D-Ti implant plates before and after electrochemical anodization is shown in Figure 3 (a–c). As seen in the images, 3D-Ti is covered with microspheres possessing variable diameters ranging from *5–30* μm resulting from incomplete melting of the Ti alloy powder used during the SLM process[22] . It is important to state that the fabricated discs were subjected to extensive sonication prior to further processing to remove any loosely attached spheres and the remaining microspheres were firmly attached to the surface as we previously confirmed.[22,24]

The surface topography of selected TNTs-3D-Ti (anodized at 60 V), presented in SEM images in Figure 3 (d–f), revealed a typical array of vertically aligned TNTs structures covering the whole surface including the microspheres and underlying surface. The random cracks are observed across the entirety of the TNTs surface as a result of the mechanical expansion during the growth of the titanium oxide (TiO_2) layer initiated by the electrochemical anodization process. The images confirm that the microspheres and TNTs films with these cracks were stable and endured the conditions of the electrochemical anodization process and following sonication. After fabrication of TNTs, the surface of the TNTs-3D-Ti discs were coated with a layer of gallium nitrate for enhanced antibacterial activity. As observed in Figure 3 (g-i), the Ga^{3+} layer completely covered the TNTs surface, confirming successful coating of the antibacterial agent.

The chemical composition of the surface of fabricated 3D-Ti and TNTs-3D-Ti discs was analyzed by using EDX, as shown in Figure 4 (a-c). Typical peaks corresponding to Ti6Al4 V alloy are displayed in spectra obtained from all samples. After anodization, a prominent oxygen peak was observed as a result of TiO_2 layer (i.e., TNTs) formation on TNTs-3D-Ti, Figure 4b. In addition, a Ga peak appeared in spectra obtained for Ga-TNTs-3D-Ti after gallium nitrate coating, confirming successful coating as seen in Figure 3c. These results were also confirmed by XRD analysis, Figure 4 (d–f), in which anatase TiO_2 peaks (JCPDS 21-1272) appeared after anodization and a peak corresponding to gallium oxide appeared in Figure 3f confirming the deposition of gallium on the surface (JCPDS 06-0180).

Water contact angle (WCA) measurements on 3D-Ti surfaces confirmed their hydrophobicity with a WCA of 133 ± 1°, as presented in Figure 4g. After anodization, TNTs-3D-Ti surface showed super-hydrophilic properties as a result of TNTs formation, which is in agreement with previous reports,[22,25] Figure 4h. At the same time, the deposition of Ga^{3+} layer did not change the hydrophilic properties of the TNTs-3D-Ti surface with the WCA estimated to be < 10°, as shown in Figure 4i. Notably, surface hydrophilicity has been confirmed to reduce bacterial attachment on Ti implants.[26]

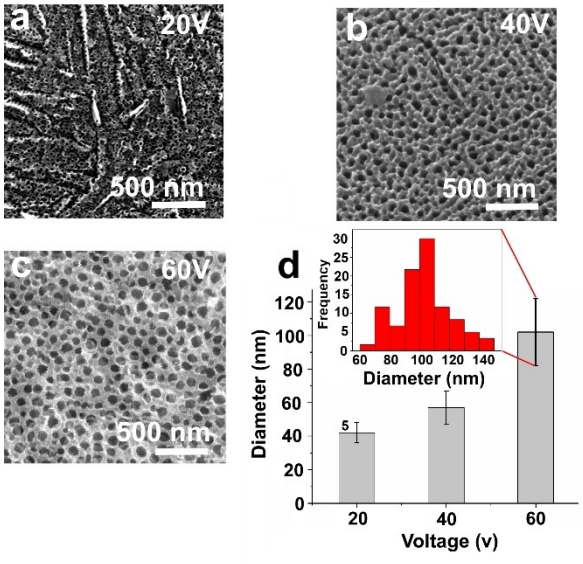

Figure 2. Effect of voltage on TNTs diameter. (a–c) High resolution SEM images showing TNTs formed under different applied voltage (20 V, 40 V and 60 V) and (d) influence of voltage on the diameter of TNTs (Values are expressed as the mean ± SD*)*, inset showing size distribution of TNTs diameters prepared at 60 V.

Gallium coating and *in-vitro* release from Ga-TNTs-3D-Ti implants

In-vitro Ga^{3+} release from Ga-TNTs-3D-Ti was assessed following incubation in PBS at 37 °C for 5 days. The typical release kinetics are presented in Figure 5. The overall Ga^{3+} release is shown to have two characteristic patterns: 1) a burst release during the first 6 h and 2) slow release over many days. A burst release pattern was observed for the initial 6 h incubation as a result of the rapid dissolution of the gallium nitrate layer covering the top surface (Figure 5b). After that, a slower release pattern was achieved with zero order kinetics due to the dissolution of Ga^{3+} trapped inside the TNTs structures. The higher Ga^{3+} release rate (~40 μg/h) at an early stage is particularly beneficial for fast eradication of bacteria at the surgical site in order to prevent possible bacterial infection that might occur either on the implant surface or in the nearby tissues within the first few hours of the implant life. At the same time, the slow release (~ 3 μg/h) over following days after surgery can provide enduring bactericidal activity, preventing potential infections.

To verify the dissolution pattern of Ga^{3+} layer in physiological conditions, the prepared samples were collected at

© 2021 Wiley-VCH GmbH

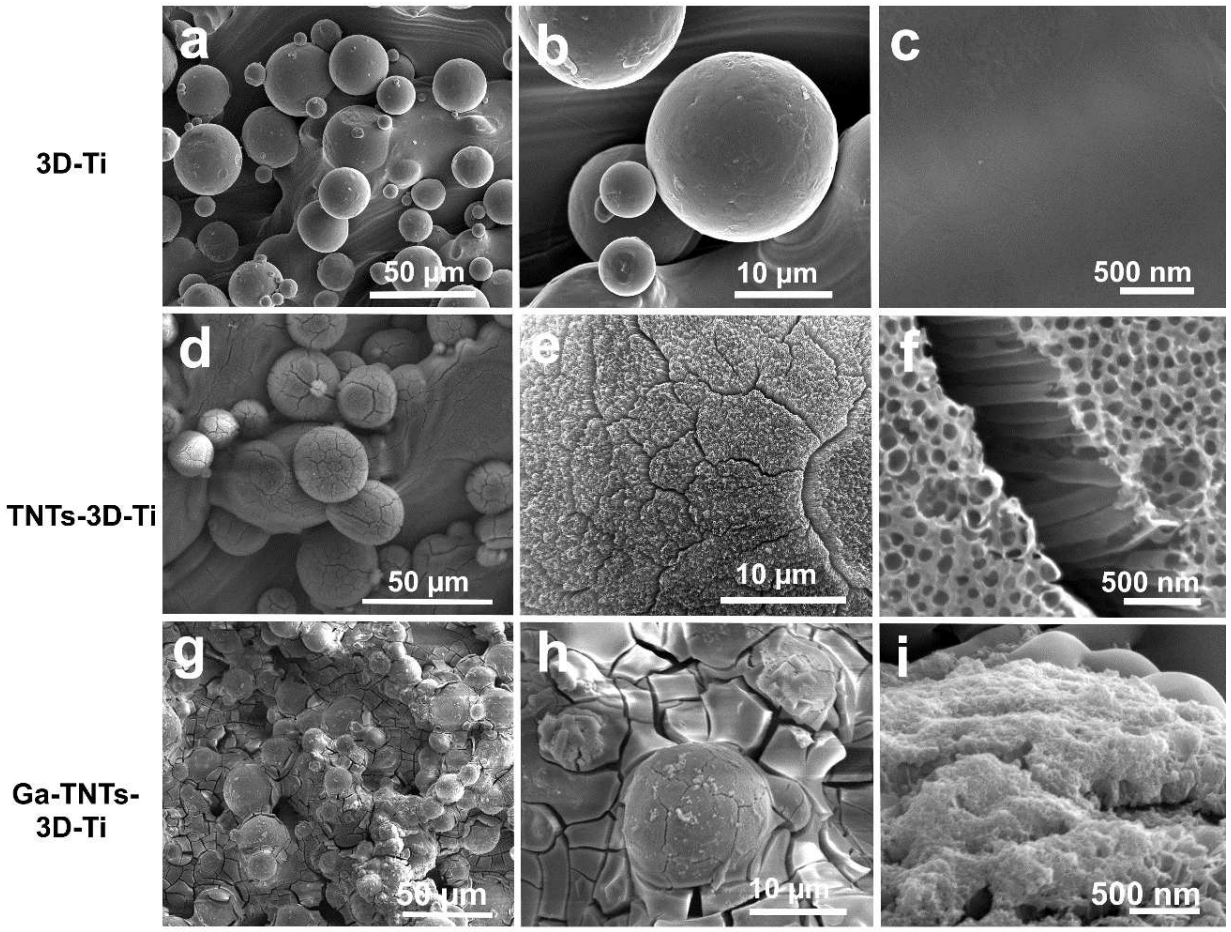

Figure 3. SEM images showing (a-c) the top surface of 3D-Ti, (d–f) TNTs-3D-Ti with arrays of titania nanotubes generated after electrochemical anodization of 3D-Ti and (g–h) Ga-HT-TNTs-3D-Ti with Ga^{3+} layer covering the whole surface. Images confirm the microstructure stability after both electrochemical anodization. (TNT: titania nanotubes, Ga: gallium).

different time points (3 and 5 days) after immersion in PBS at 37 °C and imaged using SEM, as presented in Figure 5c. SEM images clearly revealed partial dissolution of the gallium nitrate layer after 3 days, evidenced by the partial exposure of the surface TNTs. On day 5, the gallium nitrate layer was almost completely dissolved, virtually exposing the TNTs surface, as shown in Figure 5d. Only a few crystals were remaining, as denoted by the red arrows in Figure 5d. Thus, the gallium nitrate coating on modified Ti implants is expected to provide a sufficient concentration of Ga^{3+} to kill bacteria within the first few days. Following the complete dissolution of gallium nitrate layer, it is expected that the TNTs will be exposed to directly physically interact with bone cells and any remaining bacteria.

The influence of micro/nano surface topography on MG-63 viability, proliferation, and morphology

To test our hypothesis that 3D-Ti surfaces possessing TNTs with optimized diameters of ~100 nm can prevent bone cell overgrowth through excessive cell attachment and proliferation, we examined the viability and proliferation of MG-63 human osteoblastic cells on 3D-Ti and TNTs-3D-Ti discs at 1, 4 and 7 days of culture, as shown in Figure 6. Since the gallium nitrate layer dissolved within 5 days in physiological buffer, as confirmed during the *in-vitro* release study, only Ga^{3+} free samples were investigated. The cytotoxicity of Ga^{3+} ions toward human cells was previously studied for applications where Ga^{3+} can potentially make direct or indirect contact to biomaterials or human tissues. Results showed that Ga^{3+} possess no cytotoxic effect except when used in concentrations above 100 µM, which is much higher than the amount used in our experiments.[27] In addition, Ga^{3+} is currently approved by the Food and Drug Administration (FDA) as an anti-tumor and anti-hypercalcemia drug.[28]

As indicated in Figure 6a, no significant difference in cell viability was observed at day 1 between 3D-Ti and TNTs-3D-Ti. However, on days 4 and 7, the cell viability on TNTs-3D-Ti was significantly ($p < 0.0001$) reduced compared to the 3D-Ti. TNTs-3D-Ti did not show substantial cell growth at 4 and 7 days of incubation, suggesting that it might slow or hinder MG-63 cell growth. Previous studies showed that TNTs with a diameter

© 2021 Wiley-VCH GmbH

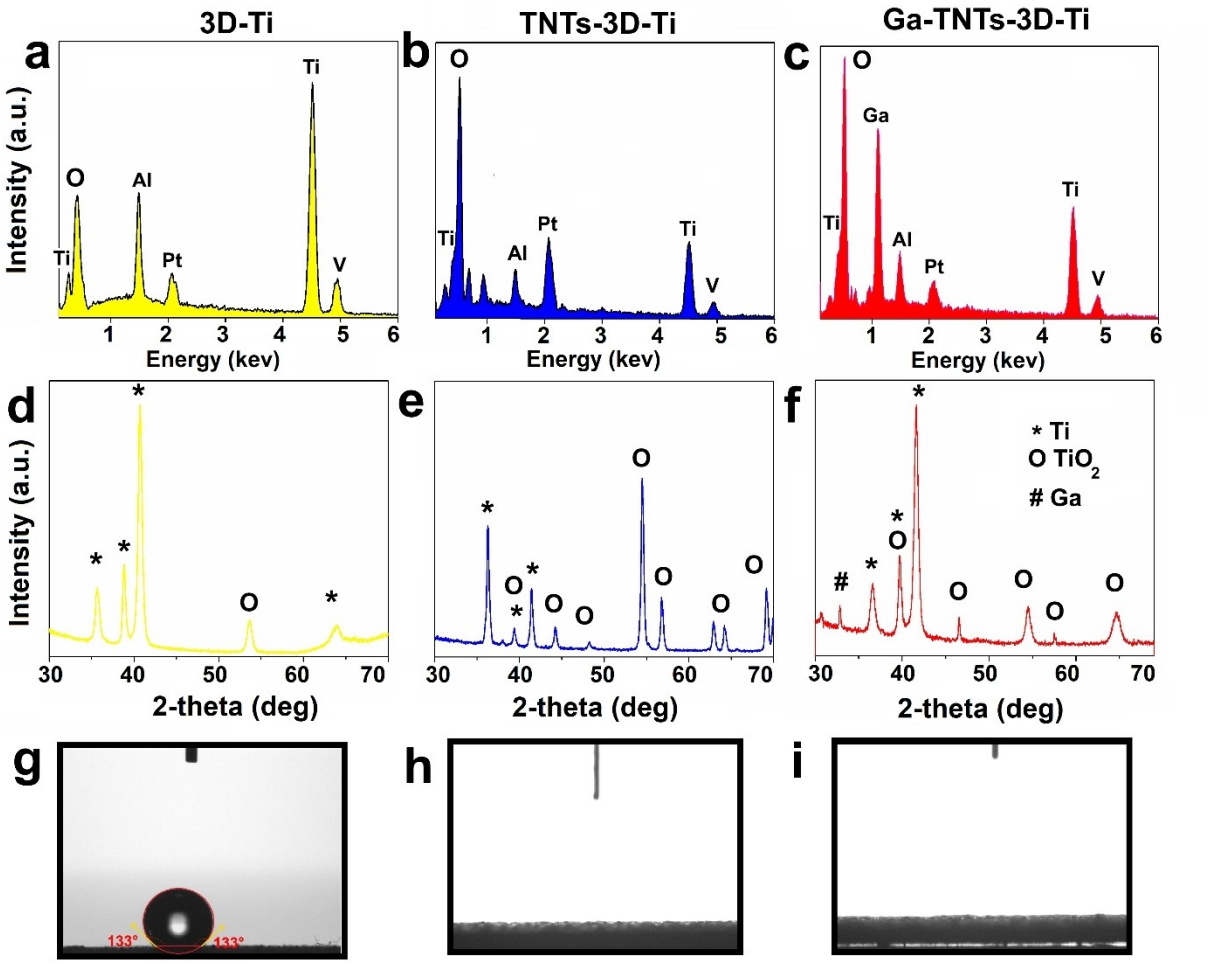

Figure 4. Characterization and surface properties of 3D-Ti, TNTs-3D-Ti and Ga-TNTs-3D-Ti. (a–c) EDX spectra, (d–f) XRD patterns with peaks corresponding to Ti, anatase TiO_2 and Ga^{3+} layer, and (g–i) wetting properties of each respective surface as confirmed by water contact angle (WCA). (TNT: titania nanotubes. Ga: gallium)

$>$90 nm could impair cell spreading and adhesion due to the inhibition of integrin clustering and reduction of focal adhesion contact point formation.[5,29] Next, cytotoxicity of the fabricated Ti implants was assessed toward MG-63 cells as a function of their cell membrane integrity. As was similarly observed from the results of the MTS assay, Figure 6b shows no significant difference between LDH release from cells attached on 3D-Ti and TNTs-3D-Ti at day 1. However, at longer incubation times, TNTs-3D-Ti showed a significant ($p < 0.05$) increase of cytotoxicity toward MG 63 cells compared to the glass control. After 4 and 7 days, cells cultured on TNTs-3D-Ti released a significantly higher amount of LDH compared to 3D-Ti and glass, indicating cell membrane damage to attached cells, which agrees with the lower cell viability observed from MTS assay results.

Live/dead fluorescent staining was then applied to directly confirm cell viability and attachment density at 1-, 4- and 7-days incubation (Figure 6c). After 24 h, the percentage of viable cells on 3D-Ti was approximately 25–30% higher than on TNTs-3D-Ti. There was a significant ($p < 0.0001$) increase in the number of viable cells observed on 3D-Ti at day 7 (Figure 6d). A similar trend was observed for cell density (cell number/cm^2), Figure 6e, in which the cell density on TNTs-3D-Ti was significantly lower ($p < 0.0001$) than on 3D-Ti after 7 days of culture. The density increased significantly on 3D-Ti at day 7 compared to days 1 and 4, while cell numbers remained relatively unchanged on TNTs-3D-Ti over the course of 7 days. All these data confirm that the fabricated TNTs with tube diameters ~100 nm can significantly reduce bone overgrowth on the surface compared to the smooth surface of 3D-Ti.

Investigation of the changes to the cell cytoskeleton by fluorescent labelling of F-actin revealed obvious deformation of the actin network structure of cells attached on TNTs-3D-Ti surfaces (Figure 6c, last column). Quantification of the focal adhesion sites by labelling of vinculin further showed MG-63 cells on 3D-Ti having a higher number (31 ± 12) of focal adhesions compared to cells on TNTs-3D-Ti (14 ± 5 focal adhesions). The reduction in the number of focal adhesion sites on TNTs-3D-Ti can be attributed to a reduction in the number of cell anchorage sites due to the gaps corresponding to TNTs pores. This, in turn, can be translated into reduced attachment of osteoblasts on the surface, as confirmed by cell attachment and viability results (*vide supra*)[14,29b].

© 2021 Wiley-VCH GmbH

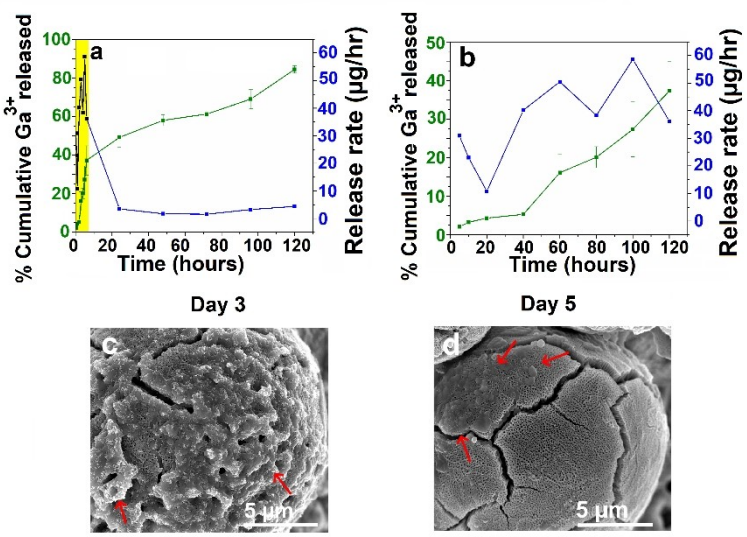

Figure 5. *In-vitro* Ga^{3+} release profiles from Ga-TNTs-3D-Ti showing % cumulative Ga^{3+} released and release rate for (a) 5 days and (b) 6 h (burst release) presenting magnified view of the yellow rectangle shown in (a), (total Ga^{3+} ~683 µg/disc). (c–d) SEM images showing dissolution of the gallium nitrate layer after 3 and 5 days. The gallium layer dissolves gradually with the TNTs surface partially exposed after 3 days while almost all the Ga^{3+} layer was dissolved within 5 days. Red arrows denoting Ga^{3+} containing layer on surface Values are expressed as the mean ± SD for at least 3 triplicates.

Next, the impact of TNTs on cell morphology and proliferation was visually examined under high resolution SEM, as shown in Figure 7. At day 1, the few cells detected on TNTs-3D-Ti exhibited a rounded morphology and were mostly attached under the shield of the microsphere structures, Figure 7b, which serves to indicate that the TNT surface is not favored by the cells. On the contrary, MG-63 cells on 3D-Ti showed the production of numerous cell extensions, forming multiple focal adhesions on the surface, as shown in Figure 7a. After 4 days of incubation, more cells showing a polygonal shape were observed on 3D-Ti, Figure 7c. At day 7, Figure 7e and f show a high density of cell spreading on 3D-Ti in contrast to TNTs-3D-Ti where only a few rounded cells were detected, as shown by the red arrows.

Based on the above results, we can conclude that the nanoporous structures of TNTs-3D-Ti did not support cell attachment. As a result, TNTs-3D-Ti could be potentially used for temporary fracture fixation to reduce bone cell overgrowth on the implant surface.[30] Another potential application of TNTs-3D-Ti surface is that they may hamper the growth of cancer cells, thus, they can be placed at the cancer site to provide temporal support and anti-cancer drug release, as we showed before. The implants can be subsequently removed easily after cancer treatment to allow the healthy bone tissue to regenerate.[22,31] It is important to note that this application will need further studies to be confirmed.

Antibacterial performance of Ga^{3+} coated (Ga-TNTs-3D-Ti) implants

To evaluate the antibacterial activity of Ga-TNTs-3D-Ti surfaces toward *S. aureus* and *P. aeruginosa*, standard plate count techniques were employed to assess CFU mL^{-1} following a 5 h bacterial incubation. Ga-TNTs-3D-Ti showed 100% eradication of both bacterial strains as compared to polystyrene and Ga^{3+} free TNTs-3D-Ti surfaces as control substrata, Figure 8a. Owing to the structural similarity between Ga^{3+} and iron (Fe), bacterial cells uptake Ga^{3+} instead of Fe which results in inhibition of Fe-dependent oxidation and reduction reactions essential for bacterial DNA synthesis, ultimately causing bacterial cell death.[12c] Notably, Ga^{3+} can also enhance osteoblast growth and inhibit bone breakdown. These characteristics make Ga^{3+} a potential candidate for coating additives and composite materials that simultaneously protect against bone infections while promoting bone healing.[11a,12c,d]

The bactericidal activity of Ga^{3+} ions released during the *in-vitro* experiments was also evaluated. Solutions containing released Ga^{3+} ions were collected after surfaces had been maintained in PBS for 5 days. Aliquots of Ga^{3+} containing physiological buffer was then incubated with *S. aureus* and *P. aeruginosa* bacterial suspensions. A significant reduction ($p < 0.0001$) of bacterial cells was observed, as shown in Figure 8b, confirming the antibacterial efficacy of dissolved Ga^{3+}. Based on the Ga^{3+} release pattern and its significant antibacterial activity, it is expected that Ga^{3+} will be effective against bacterial infection arising during the surgical procedure or after implant insertion from infected wounds or haematogenous seeding within the patient's body.[32]

© 2021 Wiley-VCH GmbH

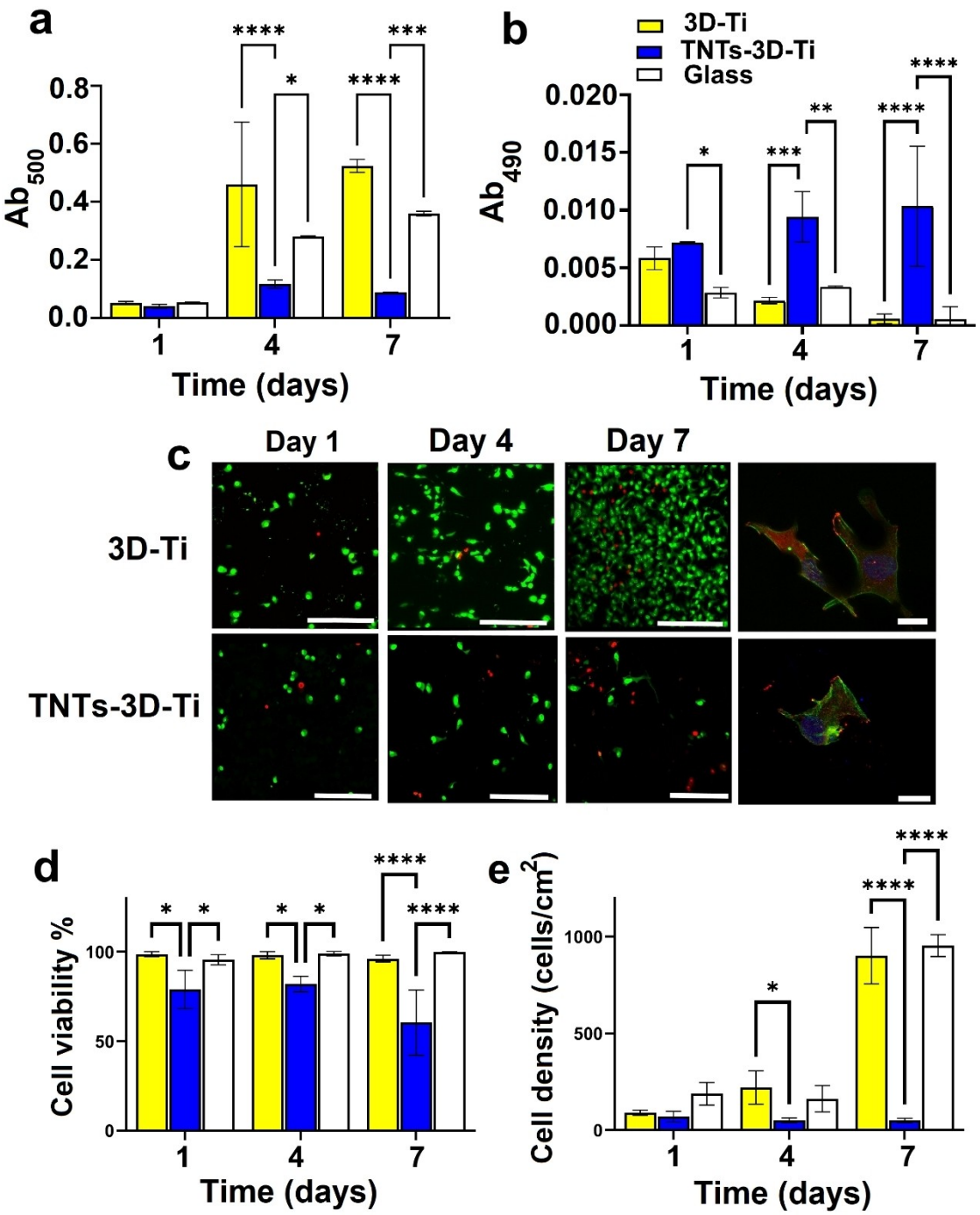

Figure 6. The viability and attachment density of osteoblast-like MG-63 cells after 1-, 4- and 7-days incubation on 3D-Ti and TNTs-3D-Ti in comparison to the control group (glass). (a) MTS assay showing cell viability on days 1, 4 and 7, (b) LDH release from MG-63 cells (normalized with cells numbers) after 1, 4 and 7 days, (c) *First three columns*, representative images of live/dead staining of MG-63 (live cells, red; dead cells, green). Scale bars = 200 μm, *last column*: confocal images showing cytoskeletal morphology and distribution of focal adhesion sites in MG-63 after 4 days of incubation. Phalloidin labelled F-actin (green), Alexa Fluor 594 labelled vinculin staining for the observation of focal adhesion (red) and TO-PRO-3 nuclear stain (blue) are shown. Scale bars = 20 μm. (d) cell viability (quantified by calculating live and dead cell numbers from the confocal images, cell viability (%) = number of live cells/number of total cells × 100 %), and (e) Cell density. Values are expressed as the mean ± SD for at least 3 replicates. Statistically significant differences are labelled as *: $p < 0.05$; **: $p < 0.01$; ***: $p < 0.001$, ****: $p < 0.0001$. (TNTs: titania nanotubes)

After the dissolution of the gallium nitrate layer, TNTs will be exposed to the surrounding environment inside the body. Thus, we then examined TNTs generated on 3D-Ti for their potential physical antibacterial activity toward *S. aureus* and *P. aeruginosa*. The TNTs-3D-Ti surfaces were incubated with bacteria for 18 h and then the bacterial attachment and viability on surface were assessed using CLSM. Fluorescence microscopy was used in comparison to plate count techniques to assess the

© 2021 Wiley-VCH GmbH

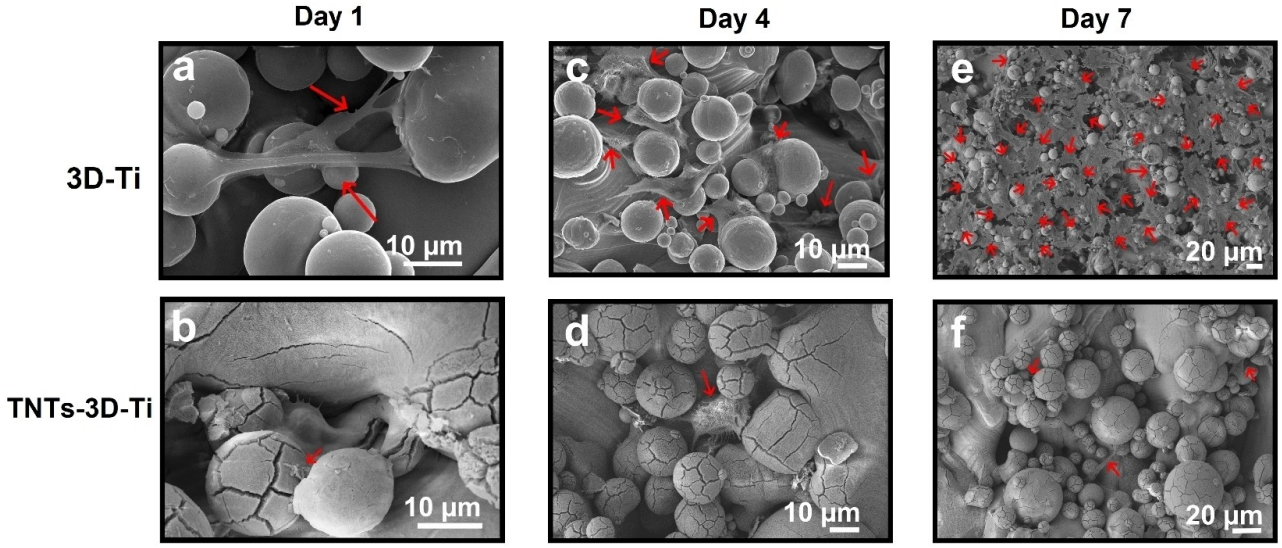

Figure 7. The morphology of MG-63 cells grown on 3D-Ti and TNTs-3D-Ti. High resolution SEM images showing the attachment and spreading of MG-63 osteoblast-like cells (indicated by the red arrows) with only a few cells attached on TNTs-3D-Ti (TNTs: titania nanotubes).

physical antibacterial action of surface nanostructures by direct observation of cell attachment and membrane integrity. Fluorescent micrographs of the bacterial attachment and proportion of live *vs* dead bacteria, as determined by live/dead staining using Syto9 (green, viable) and propidium iodide (red, non-viable) are shown in Figure 8c. Bacterial attachment, as calculated from CLSM images, show no significant difference between attachment of *S. aureus* to 3D-Ti and TNTs-3D-Ti; however, TNTs-3D-Ti experienced significantly ($p < 0.0001$) reduced levels of *P. aeruginosa* attachment with $\sim 16\times10^3 \pm 11\times10^3$ cells/mm^2 compared to 3D-Ti with $\sim 58\times10^3 \pm 16\times10^3$ attached cells/mm^2, Figure 8d.

The ability of the surface topography to physically inactivate bacteria significantly varied according to bacterial strain. TNTs-3D-Ti displayed high antibacterial efficiency against *P. aeruginosa* cells compared to *S. aureus*. This variation in antibacterial activity could be attributed to the difference in structure and thickness of the bacterial envelope between *S. aureus* (gram positive) and *P. aeruginosa* (gram negative). Gram negative bacteria are surrounded by a thin outer membrane made of lipopolysaccharide which can be easily damaged, causing bacterial death.[33] Despite the lack of such membrane in Gram positive bacteria, they are encapsuled by several layers of peptidoglycan which are ~5 times thicker than that of gram-negative bacteria. The presence of this stiff peptidoglycan layer protects *S. aureus* against the physical damage induced by TNTs.[33] In addition, both *S. aureus*. and *P. aeruginosa* appeared deformed on TNTs-3D-Ti compared to 3D-Ti as shown in SEM images, Figure 9.

Overall, the results confirm the significant influence of TNTs on the degree of bacterial retention, which was dependent on the bacterial strain (i.e., more obvious for *P. aeruginosa* than *S. aureus*). Accordingly, it can be concluded that TNTs-3D-Ti could relatively reduce the occurrence of bacterial attachment and kill bacteria that do attach on implants surface compared to smooth 3D-Ti surface.

Conclusion

The fabrication of 3D-printed Ti implants with arrays of TNTs by combination of selective laser melting and electrochemical anodization followed by Ga^{3+} coating was successfully demonstrated as a new concept proposed for a short-term implant application with enhanced bactericidal efficacy and reduced bone cell attachment. Our results showed that TNTs with tailored pore diameters (~100 nm) can be used to control the attachment and overgrowth of bone cells on the surface of the implant. This structural property makes them suitable for application as a temporary implant material intended to be removed from the body.

Superior antibacterial activity of the fabricated implant models was successfully achieved by coating of Ga^{3+} as a non-conventional antibacterial agent that demonstrated the ability to provide sufficient concentrations of Ga^{3+} able to effectively eradicate 100% of bacteria. Interestingly, the physical (mechano-)bactericidal activity of TNTs was significantly dependent on the bacterial strain; Ga^{3+} free 3D-Ti-TNTs surfaces could significantly kill *P. aeruginosa* while simultaneously reducing their surface attachment, in contrast to *S. aureus*, which were more resistant to the mechanical bactericidal action.

The presented work confirms the potential of a new generation of low-cost, removable implants whose performance can be enhanced by dual combination of surface topography and drug-releasing functionality that enables control of bone cell response while effectively inhibiting bacterial colonization. Nevertheless, further studies are required for optimization of cellular response and tuning of the antibacterial performances

© 2021 Wiley-VCH GmbH

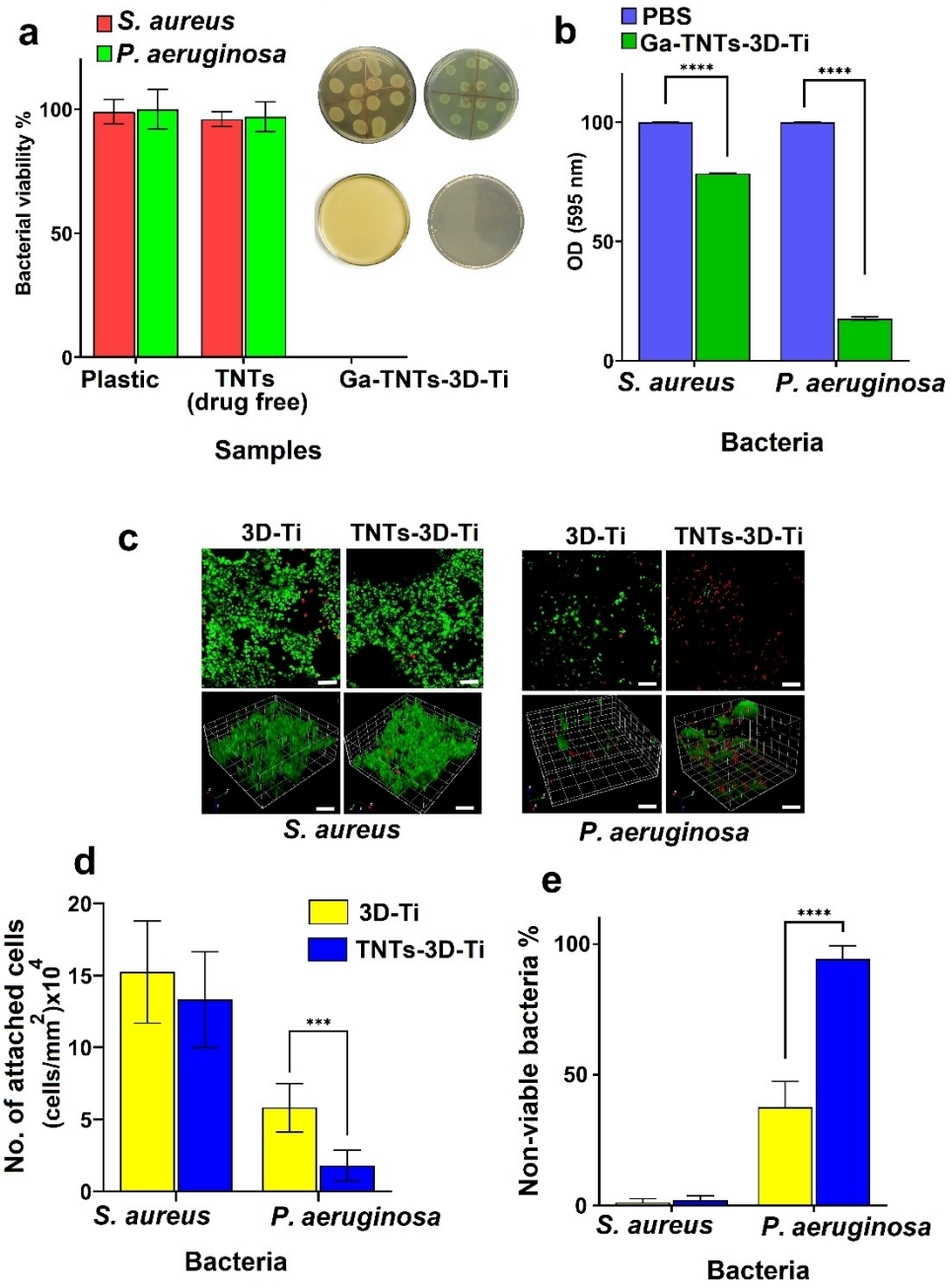

Figure 8. Antibacterial activity of Ga^{3+} coated discs and TNTs showing (a) 100% bacterial eradication on Ga-TNTs-3D-Ti compared to controls. (b) Significant reduction of bacterial proliferation when exposed to solutions containing the *in-vitro* release of Ga^{3+} in PBS for 5 days against both bacterial strains. (c) Representative CLSM micrographs of *S. aureus* and *P. aeruginosa* bacterial growth (upper raw), 3D reconstructions of the CLSM z-series (bottom raw), scale bars = 10 μm. (d) Attachment of *S. aureus* and *P. aeruginosa* on 3D-Ti and TNTs-3D-Ti and (e) antibacterial activity of 3D-Ti and TNTs-3D-Ti against both bacterial strains. Values are expressed as the mean ± SD for at least 3 replicates. Statistically significant differences are labelled as *: $p < 0.05$; **: $p < 0.01$; ***: $p < 0.001$, ****: $p < 0.0001$. (TNTs: titania nanotubes)

of fabricated 3D-printed implantable Ti materials; however, we have successfully validated their potential to be transformed into the next stage of *in-vivo* and clinical studies.

Experimental Section

Fabrication of 3D Ti implants

Ti6Al4 V powder (Titanium grade 5, TLS Technik GmbH & Co. Spezialpulver, Germany) was used to fabricate 3D-Ti discs of size 1.5 × 1.5 cm^2 using SLM machine (ProX 200 Production 3D Printer, Phenix Systems PXM (USA), equipped with a 300 W Laser (1070 nm at 50% power)) under inert argon atmosphere. Details of the

© 2021 Wiley-VCH GmbH

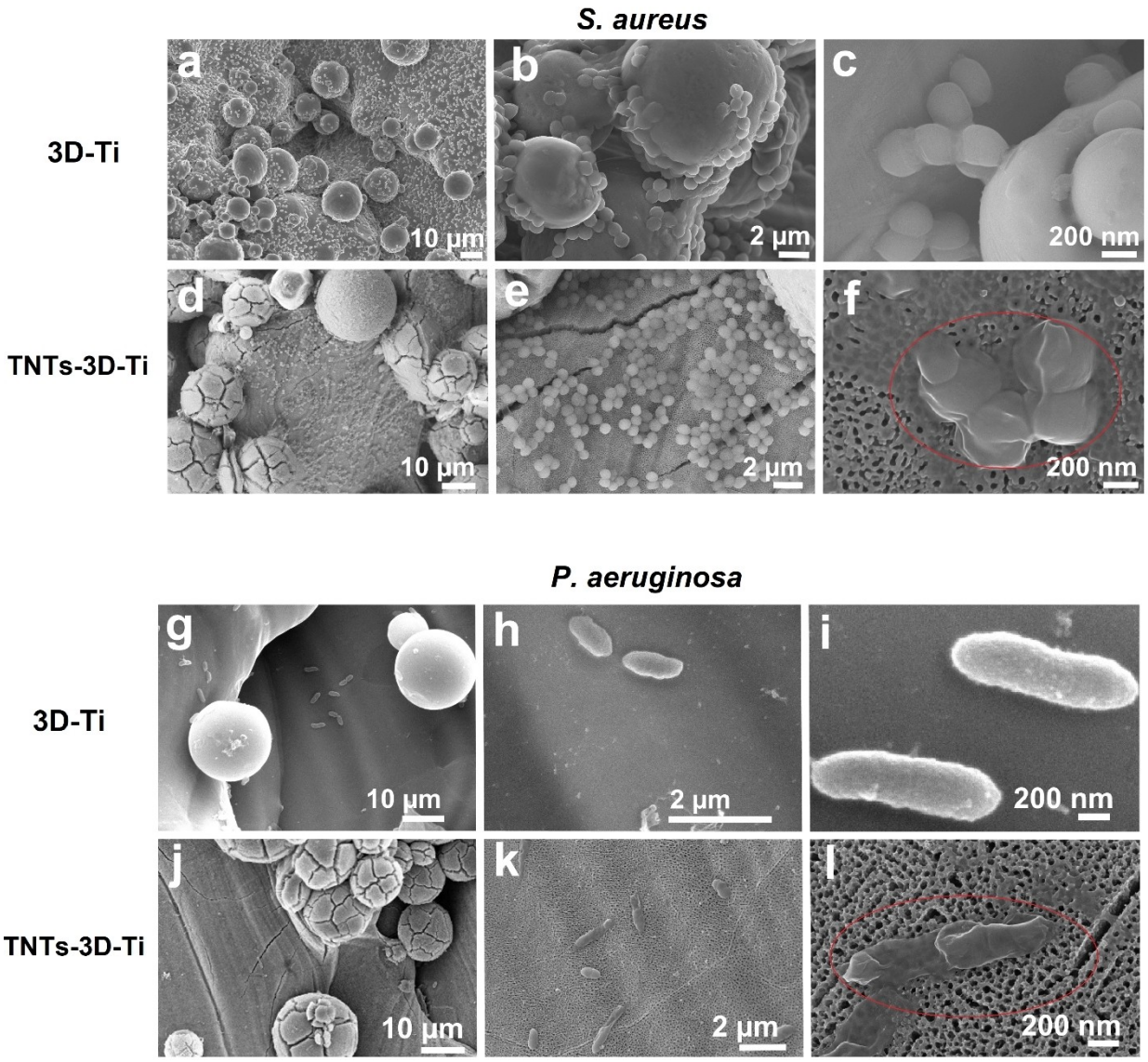

Figure 9. Attachment pattern and morphology of *S. aureus* (a-f) and *P. aeruginosa* (g-l) on 3D-Ti and TNTs-3D-Ti surfaces. SEM images showing the morphology of bacterial cells that appear healthy on 3D-Ti, in contrast to TNTs-3D-Ti in which bacterial cells appear deformed, as marked by red circles. (TNTs: titania nanotubes)

fabrication and the average diameter of particles were reported in our previous study.[22] After fabrication, the discs were cleaned by sonication in acetone for 10 min to eliminate any loosely attached powder particles. The resulting discs will be referred to as "3D-Ti".

Titania nanotubes fabrication on 3D-Ti

Titanium nanotubes (TNTs) were generated on the surface of 3D-Ti discs through electrochemical anodization (EA) process under a temperature-controlled system designed in our laboratory as described elsewhere.[22] Briefly, 3D-Ti discs were anodized in ethylene glycol electrolyte solution containing NH_4F (0.1 M), lactic acid (1.5 M) and water (5% w/w), (Chem-Supply, Australia) at 20, 40 or 60 V for 15 min with constant stirring at 60 °C. The applied voltage was controlled by programmable power supply (Agilent, USA) and current change was recorded using the LabView program (National Instruments). After anodization, the 3D-Ti discs with TNTs on top (TNTs-3D-Ti) were sonicated in Milli-Q water for 5 min to remove any remaining chemicals.

All samples (*i.e.*, 3D-Ti and TNTs-3D-Ti) were placed in Milli-Q water for 2 weeks prior to bacterial studies to ensure the complete removal of any residual chemicals from the fabrication process.

Gallium nitrate coating onto TNTs-3D-Ti

Gallium nitrate was coated on TNTs-3D-Ti by application of 10 µL of gallium nitrate solution (10 mg mL^{-1}) on the surface and leaving to dry under vacuum for 1 h at room temperature to remove air gaps inside the TNTs. Each disc was loaded with 2500 µg of gallium nitrate (equivalent to ~683 µg of Ga^{3+}/disc) by repeating this step 25 times.

© 2021 Wiley-VCH GmbH

Characterization

High resolution images of the fabricated Ti implants (3D-Ti and TNTs-3D-Ti) were recorded using focused ion beam (FIB)-scanning electron microscopy (SEM) (FEI Helios Nanolab 600 Dual Beam, Thermo Fisher Scientific, Australia). The chemical composition of the surface was analyzed using energy-dispersive X-ray spectroscopy (EDX, Oxford Ultim Max Large Area SDD EDS detector, Oxford instruments, USA). All substrata were coated with platinum (5 nm) prior to imaging. X-ray diffraction spectra (XRD, Rigaku MiniFlex 600, Japan) were obtained to show crystallinity of the surface micro-nano structures at a scanning rate of 10 degrees per min using $Cu_{K\alpha}$ radiation over the range of 30–80°. Water contact angle (WCA) measurements were also recorded using sessile drop method at room temperature using a tension theta optical tensiometer (KSV instruments, Finland). Three samples were tested with at least three separate measurements were taken for each one. WCA was measured over 10 seconds using 5 μl of Milli-Q water.

In-vitro Ga^{3+} release

The *in-vitro* Ga^{3+} release was assessed by placing gallium nitrate coated discs (Ga-TNTs-3D-Ti) in 4 mL of PBS (pH 7.4) at 37 °C for 5 days. At a predetermined time, 400 μL of solution containing Ga^{3+} was collected and replaced with fresh PBS to maintain sink conditions.[34]

All collected release samples were stored at 4 °C until further analysis. Gallium content was analyzed using inductively coupled plasma mass spectrometry (ICP-MS Triple Quad, Agilent 8900, USA). Prior to analysis, all samples were diluted 100 times with 2% HNO_3 and then filtered with 0.22 Millipore filter prior to analysis. A calibration curve was constructed using ICP standard solution for gallium. TNTs-3D-Ti discs (*i.e.*, Ga^{3+} fee) were also placed in PBS as a blank under the same conditions. All experiments were repeated in triplicates and the data were analyzed for statistical significance.

Cell culture

Human osteosarcoma (osteoblast-like) MG-63 cells were purchased from Sigma-Aldrich (USA). Cells were cultured in 75 cm^2 cell culture (T75) flasks with Dulbecco's Modified Eagle Medium with GlutaMAX™ (Life Technologies, Inc.), supplemented with 10% fetal bovine serum, 1% Penicillin-Streptomycin (Sigma) at 37 °C in a humidified atmosphere with 5% CO_2. Cells were passaged for subculture when the cell density achieved 90% confluency. Prior to cell seeding, Ti discs and glass slides (positive control groups) were sterilized with 70% (v/v) ethanol for 10 minutes and washed twice with sterile PBS then allowed to dry overnight. MG-63 cells were subsequently seeded on the samples at a density of 2×10^4 cells cm^{-2} and incubated at 37 °C in a humidified atmosphere with 5% CO_2. The cell density was calculated using a hemocytometer.

Cell proliferation

Cell proliferation was studied using 3-(4,5-dimethylthiazol-2-yl)-5-(3-carboxymethoxyphenyl)-2-(4-sulfophenyl)-2 h tetrazolium (MTS) assay. Samples were collected after 1, 4 and 7 days of incubation and gently washed twice with PBS buffer to remove unattached cells. Afterward, the samples were transferred to a sterile well plate and incubated in DMEM with 20% (v/v) MTS reagent (Promega, WI, USA) at 37 °C in a humidified atmosphere with 5% CO_2 for 1.5 h. During incubation, tetrazolium salt is reduced by viable cells into a colored formazan dye. This reaction is mediated by NAD(P)H-dependent dehydrogenase enzymes in mitochondrial respiratory chain. The supernatant from each sample was then collected and the absorbance was measured at 500 nm using a POLARstar Omega microplate reader (BMG Labtech, Ortenberg, Germany).

Cytotoxicity assay

The concentration of extracellular lactate dehydrogenase (LDH) released from the cells seeded on 3D-Ti, TNTs-3D-Ti, and glass as a planar control surface was measured using UV/VIS spectrophotometry. At predetermined times 1, 4 and 7 days of incubation, 50 μL from the supernatant of each sample were collected and incubated for 30 min at room temperature with 50 μL of CytoTox 96® reagent (Non-Radioactive Cytotoxicity Assay Promega) in a new well-plate. The absorbance was then measured at 490 nm.

Dead/Live cell stain

After 1, 4 and 7 days of cells incubation, discs were washed twice with PBS and then covered with staining solution containing calcein AM (2 μM) and ethidium homodimer-1 (4 μM) (Life Technologies, Inc.) for 30 min in the dark at room temperature. Subsequently, the samples were rinsed and immersed in PBS followed by imaging *via* confocal microscopy (Olympus FluoView™ FV3000). Counts of live and dead cells were quantified using Matlab software, CellC. The cell viability percentage was measured as the ratio of the number of viable cells to total number of cells on the surface. At least 20 fluorescence images were taken for each sample (image size is 500 μm^2 and images were taken in a stepwise manner over the entirety of the 1 cm^2 sample) and each experiment was repeated in triplicate. Then, the cell numbers per independent replicate are averaged.

Immunocytochemistry and cytoskeleton staining

On the 4th day of cell culture, samples were washed twice with PBS and then fixed with 4% paraformaldehyde for 15 min. For permeabilization, samples were covered with 0.2% Triton X-100 for 15 min. After that, 1% bovine serum albumin (BSA) was used to block the samples for 30 min. Next, samples were incubated at room temperature with primary antibody, anti-Vinculin (mouse)(-Sigma-Aldrich) and secondary antibody, anti-Mouse IgG in 5% goat serum (Life Technologies, Inc) at room temperature for 1 h. Actin filaments and cell nuclei were stained with phalloidin (Invitrogen) for 20 min followed by TO-PRO™-3 Iodide (Invitrogen) for 30 min, respectively. Cells were imaged using confocal laser scanning microscopy (CLSM; LSM710 NLO, Carl Zeiss, Oberkochen),Germany.

SEM imaging

The morphology of cells attached on 3D-Ti and TNTs-3D-Ti was assessed using SEM. Samples were gently rinsed with Milli-Q water after incubation for 1, 4 and 7 days and fixed with 2.5% v/v glutaraldehyde (Sigma) and were then rinsed 2 times with Milli-Q water. The cells were dehydrated with ethanol at increasing concentrations (30, 50, 70, 90, and 100%v/v) for 10 min each and an additional 10 min in 100 v/v% ethanol. After that, samples were immersed in hexamethyldisilazane (HMDS) (Sigma) for 10 min. The samples were left to air-dry and then sputter-coated with 5 nm gold for imaging. High resolution images were recorded using the SEM capabilities of a Raith150 two direct write ultra-high-resolution electron beam lithography tool (Raith, GmBH) under high vacuum at an accelerating voltage of 3 kV.

© 2021 Wiley-VCH GmbH

Antibacterial activity assays

Bacterial strains and growth conditions

S. aureus ATCC 25923 was purchased from American Type Culture Collection (Manassas, VA, USA). *P. aeruginosa* (clinical isolate from a chronic rhinosinusitis patient) was obtained from Adelaide Pathology Partners (Mile End, Australia). The use of bacterial isolates was approved by The Local Institutional Human Research Ethics Committee (HREC/15/TQEH/132). Both bacterial stocks were stored at −80 °C in frozen glycerol broth. Prior to each experiment, 100 μL of the *S. aureus* and *P. aeruginosa* bacteria from stocks was plated on Tryptone Soy Agar (TSA) and Nutrient Agar (NA) plates, respectively, and grown overnight at 37 °C.

Antibacterial activity of gallium coated Ti implants

Ga^{3+} coated discs (Ga-TNTs-3D-Ti) were first sterilized under UV irradiation for 30 min before testing and placed in 24-well plate. Bacterial suspensions of either *S. aureus* or *P. aeruginosa* were prepared by resuspending a single colony of bacteria in broth medium to reach 0.5 MacFarland units (approximately 1.5×10^8 colony forming units (CFU)/mL)). The bacterial suspensions of *S. aureus* and *P. aeruginosa* were then diluted 1:100 in TSB and NA, respectively to obtain a final bacterial concentration of approximately 1.5×10^6 CFU mL^{-1}. Next, the surface of the samples was covered with 20 μL of bacterial suspension and were then incubated for 5 h at 37 °C. After 5 h, the samples were placed in 980 μL of sterilized saline and shaken together for 1 min to collect viable bacteria remaining on the surface.[35] After that, ten-fold serial dilution of collected bacterial suspension was plated onto agar plates (TSA for *S. aureus* and Cetrimide agar for *P. aeruginosa*) and then incubated for 24 h at 37 °C. Finally, CFU were counted. Ga^{3+} free samples (TNTs-3D-Ti) were also treated in the same way while empty plastic wells were used as positive controls taken as 100% viability. Thus, % bacterial cells viability was calculated based on the following formula:

$$\%\ \text{Bacterial Cell Viability} = \frac{CFUs}{CFUc}\ \text{x100}$$

Where *CFUs* is the average number of CFU recorded for each sample and *CFUc* is the average CFU for plastic

Antibacterial activity of the release solution

After 5 days of Ga^{3+} release, the release solutions were collected to assess the bactericidal action of the Ga^{3+}. For each sample, 0.5 mL of collected solution was mixed with 0.5 mL of bacterial suspension containing 10^4 CFU mL^{-1} and then incubated for 5 h. After that, 200 μL of the incubate were transferred to 96 well-plate and the optical density (OD) of the bacterial suspension was determined at 595 nm using a FLUOstar OPTIMA plate reader (BMG Labtech, Ortenberg, Germany), PBS with no bacteria was used as a blank and each experiment was repeated in triplicates followed by statistically analysis.[36]

Antibacterial activity of TNTs-3D-Ti implants

3D-Ti and TNTs-3D-Ti were immersed in 1 mL of bacterial suspension (adjusted to an OD_{600} 0.1 in nutrient broth) in sterile 12-well plates for 18 h at 27 °C in dark and static conditions. Discs were then rinsed gently with PBS and stained with Live/Dead Baclight (Invitrogen) and imaged with confocal laser scanning microscopy to detect the proportion of live/dead bacteria on the surface. Images were then analyzed using Matlab software, CellC to determine the bacterial counts. SEM imaging of samples with attached bacteria, after 18 h of incubation, were processed as described above.

Statistical analysis

All the results presented in this study were statistically treated and expressed as mean ± standard deviation (SD) of at least three independent experiments. Unpaired t-test and two-way ANOVA were used to analyze the data. The level for significance was set to $p < 0.05$ for all the comparisons.

Acknowledgements

The authors acknowledge the financial support provided to S.M. by Australian Research Council (ARC) (IH 15010003) grant, the Australian Government Training Program Scholarship, and Forrest George and Sandra Lynne Young Supplementary Scholarship. The authors acknowledge the contribution of Sandy Liao from RMIT for preparing cell cultures for this study. The authors are grateful to the School of Chemical Engineering at the University of Adelaide for support of this research. Authors gratefully acknowledge the RMIT Microscopy and Microanalysis Facility (RMMF) for providing access to their analytical instruments.

Conflict of Interest

The authors declare no conflict of interest.

Keywords: Titanium implants · additive manufacturing · 3D-printing · titania nanotubes · antibacterial · gallium

[1] E. N. Feins, Y. Lee, E. D. O'Cearbhaill, N. V. Vasilyev, S. Shimada, I. Friehs, D. Perrin, P. E. Hammer, H. Yamauchi, G. Marx, A. Gosline, V. Arabagi, J. M. Karp, P. J. del Nido, *Nat. Biomed. Eng.* **2017**, *1*, 818–825.
[2] a) N. G. Grün, P. L. Holweg, N. Donohue, T. Klestil, A.-M. Weinberg, *Innovative Surgical Sciences* **2018**, *3*, 119–125; b) E. A. Gorter, D. I. Vos, C. F. M. Sier, I. B. Schipper, *Eur J Trauma Emerg Surg* **2011**, *37*, 623–627; c) Z. Gugala, R. Lindsey, *Orthopaedic Knowledge Online Journal* **2015**, *13*, 1–20.
[3] a) S. Maher, A. Mazinani, M. R. Barati, D. Losic, *Expert Opin. Drug Delivery* **2018**, *15*, 1021–1037; b) J. Lincks, B. D. Boyan, C. R. Blanchard, C. H. Lohmann, Y. Liu, D. L. Cochran, D. D. Dean, Z. Schwartz, *Biomaterials* **1998**, *19*, 2219–2232; c) K. Rabel, R.-J. Kohal, T. Steinberg, P. Tomakidi, B. Rolauffs, E. Adolfsson, P. Palmero, T. Fürderer, B. Altmann, *Sci. Rep.* **2020**, *10*, 12810; d) Y. Hou, L. Yu, W. Xie, L. C. Camacho, M. Zhang, Z. Chu, Q. Wei, R. Haag, *Nano Lett.* **2020**, *20*, 748–757.
[4] E. A. Cavalcanti-Adam, T. Volberg, A. Micoulet, H. Kessler, B. Geiger, J. P. Spatz, *Biophys. J.* **2007**, *92*, 2964–2974.
[5] Y. He, Z. Li, X. Ding, B. Xu, J. Wang, Y. Li, F. Chen, F. Meng, W. Song, Y. Zhang, *Bioact. Mater.* **2021**.
[6] a) J. G. Lyons, M. A. Plantz, W. K. Hsu, E. L. Hsu, S. Minardi, *Frontiers in Bioengineering and Biotechnology* **2020**, *8*; b) L. Liang, P. Krieg, F. Rupp, E. Kimmerle-Müller, S. Spintzyk, M. Richter, G. Richter, A. Killinger, J. Geis-Gerstorfer, L. Scheideler, *Adv. Mater. Interfaces* **2019**, *6*, 1801720; c) D. Campoccia, L. Montanaro, C. R. Arciola, *Biomaterials* **2006**, *27*, 2331–2339.
[7] J. S. Hayes, I. M. Khan, C. W. Archer, R. G. Richards, *European cells & materials* **2010**, *20*, 98–108; materials **2010**, 20, 98–108.

© 2021 Wiley-VCH GmbH

[8] X. Li, B. Wu, H. Chen, K. Nan, Y. Jin, L. Sun, B. Wang, *J. Mater. Chem. B* **2018**, *6*, 4274–4292.
[9] a) Y. Li, Y. Yang, R. Li, X. Tang, D. Guo, Y. a. Qing, Y. Qin, *Int. J. Nanomed.* **2019**, *14*, 7217–7236; b) M. Gimeno, P. Pinczowski, M. Pérez, A. Giorello, M. Á. Martínez, J. Santamaría, M. Arruebo, L. Luján, *Eur. J. Pharm. Biopharm.* **2015**, *96*, 264–271.
[10] D. Losic, M. S. Aw, A. Santos, K. Gulati, M. Bariana, *Expert Opin. Drug Delivery* **2015**, *12*, 103–127.
[11] a) B. W. Stuart, G. E. Stan, A. C. Popa, M. J. Carrington, I. Zgura, M. Necsulescu, D. M. Grant, *Bioactive Materials* **2021**; b) D. Campoccia, L. Montanaro, P. Speziale, C. R. Arciola, *Biomaterials* **2010**, *31*, 6363–6377.
[12] a) E. Zhang, X. Zhao, J. Hu, R. Wang, S. Fu, G. Qin, *Bioact. Mater.* **2021**, *6*, 2569–2612; b) A. Cochis, B. Azzimonti, R. Chiesa, L. Rimondini, M. Gasik, *ACS Biomater. Sci. Eng.* **2019**, *5*, 2815–2820; c) L. Li, H. Chang, N. Yong, M. Li, Y. Hou, W. Rao, *J. Mater. Chem. B* **2021**, *9*, 85–93; d) L. C. S. Antunes, F. Imperi, F. Minandri, P. Visca, *Antimicrob. Agents Chemother.* **2012**, *56*, 5961–5970.
[13] D. Campoccia, L. Montanaro, C. R. Arciola, *Biomaterials* **2013**, *34*, 8533–8554.
[14] T. L. Clainche, D. Linklater, S. Wong, P. Le, S. Juodkazis, X. L. Guével, J.-L. Coll, E. P. Ivanova, V. Martel-Frachet, *ACS Appl. Mater. Interfaces* **2020**, *12*, 48272–48283.
[15] K. Gulati, M. S. Aw, D. Losic, *Nanoscale Res. Lett.* **2011**, *6*, 571–576.
[16] a) J. Ni, H. Ling, S. Zhang, Z. Wang, Z. Peng, C. Benyshek, R. Zan, A. K. Miri, Z. Li, X. Zhang, J. Lee, K. J. Lee, H. J. Kim, P. Tebon, T. Hoffman, M. R. Dokmeci, N. Ashammakhi, X. Li, A. Khademhosseini, *Mater. Today Bio* **2019**, *3*, 100024; b) C. Cai, X. Wu, W. Liu, W. Zhu, H. Chen, J. C. D. Qiu, C. N. Sun, J. Liu, Q. Wei, Y. Shi, *J. Mater. Sci. Technol.* **2020**, *57*, 51–64.
[17] S. H. Ko, H. Pan, C. P. Grigoropoulos, C. K. Luscombe, J. M. J. Fréchet, D. Poulikakos, *Nanotechnology* **2007**, *18*, 345202.
[18] a) Z. Jing, R. Ni, J. Wang, X. Lin, D. Fan, Q. Wei, T. Zhang, Y. Zheng, H. Cai, Z. Liu, *Bioactive Materials* **2021**, *6*, 4542–4557; b) D. Zhang, D. Qiu, M. A. Gibson, Y. Zheng, H. L. Fraser, D. H. StJohn, M. A. Easton, *Nature* **2019**, *576*, 91–95; c) L. Yuan, S. Ding, C. Wen, *Bioact. Mater.* **2019**, *4*, 56–70.
[19] C. Yin, T. Zhang, Q. Wei, H. Cai, Y. Cheng, Y. Tian, H. Leng, C. Wang, S. Feng, Z. Liu, *Bioact. Mater.* **2021**.
[20] a) J. Park, S. Bauer, K. von der Mark, P. Schmuki, *Nano Lett.* **2007**, *7*, 1686–1691; b) S. Minagar, J. Wang, C. C. Berndt, E. P. Ivanova, C. Wen, *J. Biomed. Mater. Res. Part A* **2013**, *101 A*, 2726–2739; c) C. von Wilmowsky, S. Bauer, R. Lutz, M. Meisel, F. W. Neukam, T. Toyoshima, P. Schmuki, E. Nkenke, K. A. Schlegel, *J. Biomed. Mater. Res. Part B* **2009**, *89B*, 165–171.
[21] M. Ribeiro, F. J. Monteiro, M. P. Ferraz, *Biomatter* **2012**, *2*, 176–194.
[22] S. Maher, G. Kaur, L. Lima-Marques, A. Evdokiou, D. Losic, *ACS Appl. Mater. Interfaces* **2017**, *9*, 29562–29570.
[23] K. Gulati, A. Santos, D. Findlay, D. Losic, *J. Phys. Chem. C* **2015**, *119*, 16033–16045.
[24] S. Maher, A. R. Wijenayaka, L. Lima-Marques, D. Yang, G. J. Atkins, D. Losic, *ACS Biomater. Sci. Eng.* **2021**, *7*, 441–450.
[25] J. Drelich, E. Chibowski, *Langmuir* **2010**, *26*, 18621–18623.
[26] Y. Yuan, M. P. Hays, P. R. Hardwidge, J. Kim, *RSC Adv.* **2017**, *7*, 14254–14261.
[27] J.-H. Kim, S. Kim, J.-H. So, K. Kim, H.-J. Koo, *ACS Appl. Mater. Interfaces* **2018**, *10*, 17448–17454.
[28] J. Dong, D. Fang, L. Zhang, Q. Shan, Y. Huang, *Materialia* **2019**, *5*, 100209.
[29] a) B. Voltrova, V. Hybasek, V. Blahnova, J. Sepitka, V. Lukasova, K. Vocetkova, V. Sovkova, R. Matejka, J. Fojt, L. Joska, M. Daniel, E. Filova, *RSC Adv.* **2019**, *9*, 11341–11355; b) K. S. Brammer, S. Oh, C. J. Cobb, L. M. Bjursten, H. v. d. Heyde, S. Jin, *Acta Biomater.* **2009**, *5*, 3215–3223; c) Y. Q. Hao, S. J. Li, Y. L. Hao, Y. K. Zhao, H. J. Ai, *Appl. Surf. Sci.* **2013**, *268*, 44–51.
[30] a) H. A. Peterson, *Journal of pediatric orthopedics* **2005**, *25*, 107–115; b) G. Reith, V. Schmitz-Greven, K. O. Hensel, M. M. Schneider, T. Tinschmann, B. Bouillon, C. Probst, *BMC Surg.* **2015**, *15*, 96–96.
[31] G. Kaur, T. Willsmore, K. Gulati, I. Zinonos, Y. Wang, M. Kurian, S. Hay, D. Losic, A. Evdokiou, *Biomaterials* **2016**, *101*, 176–188.
[32] P. Izakovicova, O. Borens, A. Trampuz, *EFORT Open Reviews* **2019**, *4*, 482–494.
[33] a) T. J. Silhavy, D. Kahne, S. Walker, *Cold Spring Harbor Perspect. Biol.* **2010**, *2*, a000414; b) C. E. Harper, C. J. Hernandez, *APL Bioeng* **2020**, *4*, 021501–021501.
[34] M. Gibaldi, S. Feldman, *J. Pharm. Sci.* **1967**, *56*, 1238–1242.
[35] W. Zhang, S. Zhang, H. Liu, L. Ren, Q. Wang, Y. Zhang, *J. Mater. Sci. Technol.* **2021**, *88*, 158–167.
[36] a) D. Gan, T. Xu, W. Xing, X. Ge, L. Fang, K. Wang, F. Ren, X. Lu, *Adv. Funct. Mater.* **2019**, *29*, 1805964; b) D. Gan, W. Xing, L. Jiang, J. Fang, C. Zhao, F. Ren, L. Fang, K. Wang, X. Lu, *Nat. Commun.* **2019**, *10*, 1487.

Manuscript received: September 2, 2021
Revised manuscript received: September 29, 2021
Accepted manuscript online: October 4, 2021
Version of record online: ■■, ■■■

© 2021 Wiley-VCH GmbH

FULL PAPERS

The next generation of short-term removable 3D-printed implants: 3D-printed titanium implants are fabricated by combining selective laser melting (SLM) and electrochemical anodization (EA) to generate unique hierarchical micro-nano surface features, which makes them outstanding candidate for pediatric orthopedic implants by controlling bone cells growth while inhibiting bacterial infection.